

# Effect of FeO/SiO<sub>2</sub> Ratio, Al<sub>2</sub>O<sub>3</sub>, and CaO Content on Viscosity and Ionic Structure in FeO–SiO<sub>2</sub>–Al<sub>2</sub>O<sub>3</sub>–CaO–MgO–Cr<sub>2</sub>O<sub>3</sub> Melts



JENNY ISAKSSON, ANTON ANDERSSON, ANDREAS LENNARTSSON, FRANCIS GYAKWAA, QIFENG SHU, and CAISA SAMUELSSON

Pyrometallurgical copper extraction generates between 2.2 and 3.0 tons of slag per ton of copper. Copper smelting slag usually contains between 1 and 2 wt pct Cu, resulting in a substantial amount. Effective slag cleaning is critical to enhance copper recovery, often achieved through settling where entrained droplets separate from the slag. Controlling slag viscosity is vital, directly influencing the settling rate and overall efficiency. The literature has limited data on the correlation between viscosity, ionic structure, and the molar ratio of (Al<sub>2</sub>O<sub>3</sub> + SiO<sub>2</sub>)/MO (MO represents basic oxides) of iron silicate melts. This study investigates how FeO/SiO<sub>2</sub> ratio (1.08 and 1.25 at pct/at pct), CaO content (1.2 and 12 at pct), and Al<sub>2</sub>O<sub>3</sub> content (1.4 or 5 at pct) affect the viscosity and melt structure in a FeO–SiO<sub>2</sub>–Al<sub>2</sub>O<sub>3</sub>–CaO–MgO–Cr<sub>2</sub>O<sub>3</sub> system. The study was done by synthesizing the melts, followed by water granulation. The ionic structure was analyzed using Raman spectroscopy, and the viscosity was measured using a high-temperature rheometer. The findings reveal a correlation between melt structure and viscosity, where the viscosity increased when the slag was more polymerized, having a higher content of SiO<sub>2</sub> and Al<sub>2</sub>O<sub>3</sub>. The study offers insights for optimizing slag properties in industrial settings.

<https://doi.org/10.1007/s11663-025-03510-1>  
© The Author(s) 2025

## I. INTRODUCTION

SLAG viscosity is a crucial physicochemical property in pyrometallurgical metal extraction, influencing the smelter efficiency by affecting the recovery of valuable metals and the ease of tapping. Beyond slag tapping, slag viscosity also plays a critical role in mass and heat transfer,<sup>[1,2]</sup> furnace refractory life, freeze lining on a water-cooled reactor,<sup>[3,4]</sup> and the efficiency of metal droplets settling within the slag.<sup>[5]</sup> For example, higher slag viscosity in the copper industry can lead to prolonged tapping times and reduced recovery of entrained copper droplets, highlighting the need for precise control of this property.

During copper extraction, copper is distributed as entrained droplets and dissolved copper within the slag matrix.<sup>[6]</sup> The entrained droplets can be recovered through slag-cleaning operations, such as settling processes. In these processes, the droplets settle owing to the higher specific gravity of copper/matte, accumulate at the furnace bottom, and are subsequently recovered. Effective control of slag viscosity enhances metal recovery and ensures stable operations.

Copper smelting slag is typically fayalitic (Fe<sub>2</sub>SiO<sub>4</sub>), primarily containing FeO<sub>x</sub> ( $x = 1.0–1.5$ ) and SiO<sub>2</sub>, with smaller amounts of Al<sub>2</sub>O<sub>3</sub>, CaO, MgO, and minor elements like Cu, As, Sb, Sn, and Pb.<sup>[7–11]</sup> Due to declining ore grades,<sup>[12]</sup> copper concentrates with higher impurity levels and increased gangue content are being utilized, introducing more Al<sub>2</sub>O<sub>3</sub>, CaO, and MgO into the slag. Al<sub>2</sub>O<sub>3</sub> may also enter the process through recycling streams, such as waste electrical and electronic equipment, contributing to increased Al<sub>2</sub>O<sub>3</sub> content in slag. The presence of these components influences the slag properties, including viscosity.

Several factors influence the slag viscosity, including temperature, atmosphere, composition, and melt structure. The structure of silicate-based melts is influenced by three main factors: (i) the polymerization degree of the silicate network, (ii) the fitting of certain cations like Al<sup>3+</sup>,

JENNY ISAKSSON, ANTON ANDERSSON, ANDREAS LENNARTSSON, and CAISA SAMUELSSON are with the Division of Minerals and Metallurgical Engineering, Luleå University of Technology, 97 187, Luleå, Sweden. Contact e-mail: jenny.isaksson@ltu.se FRANCIS GYAKWAA and QIFENG SHU are with the Process Metallurgy Research Unit, University of Oulu, 90014, Oulu, Finland

Manuscript submitted August 30, 2024; accepted February 25, 2025.

Article published online March 14, 2025.

and (iii) the network-breaking role of cations such as  $\text{Ca}^{2+}$  and  $\text{Mg}^{2+}$ .<sup>[13]</sup> Molten silicate oxide systems consist of three-dimensional networks of  $[\text{SiO}_4]^{4-}$  tetrahedra where there are three types of oxygen: (1) bridging ( $\text{O}^0$ ), (2) non-bridging ( $\text{O}^{1-}$ ), and (3) free ( $\text{O}^{2-}$ ).<sup>[14,15]</sup> The gradual addition of basic oxides results in the progressive breaking of the bridging oxygen and the formation of non-bridging oxygen and, subsequently, free oxygen ions. Disrupting the bond between oxygen and silicon ( $\text{Si-O-Si}$ ) results in smaller structural units in the melt, making it less polymerized and lowering the viscosity due to decreased internal friction.

Research on the effect of  $\text{FeO}/\text{SiO}_2$  ratio on the molten slag viscosity has been conducted, showing significant discrepancies. However, Chen *et al.*<sup>[16]</sup> compiled previous studies and indicated a consistent trend: viscosity increases continuously with increasing  $\text{SiO}_2$  content.<sup>[1,16-18]</sup> This trend is attributed to the silicate structure, which becomes depolymerized when the  $\text{FeO}/\text{SiO}_2$  ratio is increased, forming simpler silicate units as  $\text{FeO}$  dissociates into  $\text{Fe}^{2+}$  and  $\text{O}^{2-}$ . The free oxygen ions break the bridging oxygen in the silicate network, increasing the number of non-bridging oxygen (NBO). Park *et al.*<sup>[19]</sup> examined the effect of  $\text{Fe}/\text{SiO}_2$  ratio (wt pct/wt pct) on viscosity at a fixed  $\text{Al}_2\text{O}_3$  content in the ternary  $\text{FeO}-\text{Al}_2\text{O}_3-\text{SiO}_2$  system. The results showed that the viscosity decreased with increasing  $\text{Fe}/\text{SiO}_2$  ratio from 0.95 to 2.0. The effect was ascribed to decreased silicate sheets in the melt, forming simpler, more depolymerized silicate structures.<sup>[19]</sup>

Wang *et al.*<sup>[20]</sup> studied the effect of the  $\text{Fe}/\text{SiO}_2$  ratio (wt pct/wt pct) ranging from 0.8 to 1.2 on the viscosity of  $\text{FeO}-\text{Fe}_2\text{O}_3-\text{SiO}_2-8$  wt pct  $\text{CaO}-3$  wt pct  $\text{MgO}-3$  wt pct  $\text{Al}_2\text{O}_3$  melts, showing that the viscosity decreased with an increasing ratio. At a fixed  $\text{Fe}/\text{SiO}_2$  ratio of 1.2, the effect of  $\text{Fe}_2\text{O}_3$  content (4–12 wt pct) on viscosity was studied, showing that the viscosity increased as the  $\text{Fe}_2\text{O}_3$  content increased. At lower  $\text{Fe}/\text{SiO}_2$  ratios of 0.8 and 1.0, the viscosity showed minimum values at  $\text{Fe}_2\text{O}_3$  content of 12 wt pct. Fourier transform infrared spectroscopy (FTIR) and Raman spectroscopy showed that an increasing  $\text{Fe}/\text{SiO}_2$  ratio results in a more depolymerized network. A higher  $\text{Fe}_2\text{O}_3$  content decreased the polymerization degree at the lower  $\text{Fe}/\text{SiO}_2$  ratios and increased the polymerization degree at the higher  $\text{Fe}/\text{SiO}_2$  ratio of 1.2. The effect of  $\text{Fe}_2\text{O}_3$  on the melt structure and viscosity is explained by the amphoteric behavior of  $\text{Fe}^{3+}$ , which can be present in the network-forming tetrahedral  $[\text{FeO}_4]$  and the octahedral network-breaking form  $[\text{FeO}_6]$ .<sup>[20]</sup>

Moreover, significant work has also been done to understand the effect of  $\text{Al}_2\text{O}_3$  content on slag viscosity. Mohri *et al.*<sup>[21]</sup> demonstrated that  $\text{Al}^{3+}$  increases melt viscosity by binding  $[\text{SiO}_4]^{4-}$  monomers, forming a polymerized network structure in the ternary  $\text{N}_2\text{O}-\text{Al}_2\text{O}_3-\text{SiO}_2$  system. Kim *et al.*<sup>[22]</sup> reported a similar trend in  $\text{CaO}-\text{SiO}_2-\text{MgO}-\text{FeO}$  slags, where viscosity increased with  $\text{Al}_2\text{O}_3$  content at fixed basicity and  $\text{MgO}$  content due to gradual polymerization.

Li *et al.*<sup>[23]</sup> further demonstrated the amphoteric behavior of  $\text{Al}_2\text{O}_3$  in a  $\text{CaO}-\text{SiO}_2-\text{Al}_2\text{O}_3-\text{MgO}-\text{FeO}-\text{TiO}_2$  system. The study showed that the viscosity reached a maximum at 15 wt pct  $\text{Al}_2\text{O}_3$  and then

decreased when increasing the  $\text{Al}_2\text{O}_3$  content up to 18 wt pct. The amphoteric behavior of  $\text{Al}_2\text{O}_3$  was suggested to depend primarily on the slag composition.<sup>[23]</sup> While most studies have focused on calcium silicate-based slag systems, Wang *et al.*<sup>[24]</sup> investigated the viscosity and structure of secondary copper smelting slag in a  $\text{SiO}_2-\text{FeO}-\text{Al}_2\text{O}_3-\text{Fe}_2\text{O}_3-\text{CaO}-\text{MgO}$  system. It was observed that the viscosity increased with the  $\text{Al}_2\text{O}_3$  addition from 0 to 12 wt pct, suggesting that  $\text{Al}_2\text{O}_3$  acts as an acidic oxide in the slag system, increasing the polymerization degree of the slag.<sup>[24]</sup> Chen *et al.*<sup>[25]</sup> studied the viscosity of ferronickel smelting slag and found that increasing the  $\text{Al}_2\text{O}_3$  content raised the viscosity due to the polymerization of the silicate network. Additional studies have also focused on the  $\text{Al}_2\text{O}_3$  content in iron silicate melts, consistently suggesting that viscosity increases with increasing  $\text{Al}_2\text{O}_3$  content. However, many of these lack evaluations of the corresponding slag structure.<sup>[26-28]</sup>

The ionic structure and amphoteric behavior of  $\text{Al}_2\text{O}_3$  in silicate melts have been assigned to the coordination of  $\text{Al-O}$ , as it can form both a tetrahedral ( $\text{AlO}_4$ ) and octahedral ( $\text{AlO}_6$ ) structure.  $\text{Al-O}$  coordination would be tetrahedral in alkaline silicate melts containing  $\text{Al}_2\text{O}_3$  when the molar ratio of  $\text{Al}_2\text{O}_3/\text{MO}$  ( $\text{MO}$  represents basic oxides like  $\text{CaO}$ ,  $\text{FeO}$ , and  $\text{MgO}$ ) is less than unity. When the ratio exceeds unity, the cation would have an octahedral coordination acting like a network breaker.<sup>[29,30]</sup> The tetrahedral  $\text{Al}$ -unit can be incorporated into the silicate network, increasing the viscosity.<sup>[29]</sup> Tetrahedral units of  $[\text{AlO}_4]^{5-}$  carry a different charge than the silicate tetrahedral  $[\text{SiO}_4]^{4-}$ , necessitating the presence of cations to maintain charge balance.<sup>[31]</sup> For instance, structures such as  $[1/2\text{Ca}(\text{AlO}_4)]^{4-}$ , where  $\text{Ca}^{2+}$  ions must be close to the  $\text{Al}^{3+}$  ion.

The effect of  $\text{CaO}$  addition on viscosity has been extensively studied in iron silicate melts, with results consistently showing that increasing the  $\text{CaO}$  content reduces viscosity.<sup>[28,32-37]</sup> The underlying theory is similar to  $\text{FeO}$ :  $\text{CaO}$  dissociates into  $\text{Ca}^{2+}$  and  $\text{O}^{2-}$ , with free oxygen breaking the bridging oxygen in the silicate network, thus disrupting the structure and reducing viscosity. Isaksson *et al.*<sup>[38]</sup> showed that modifying iron silicate slag with  $\text{CaO}$  at an industrial scale reduces slag viscosity, increases the size of copper droplets, and lowers copper solubility, thereby improving the recovery of copper in a settling process.

Building on this, the present study investigates the influence of slag composition and ionic structure on the viscosity of melts relevant to pyrometallurgical copper extraction. High-temperature viscosity measurements were performed on synthetic  $\text{FeO}-\text{SiO}_2-\text{Al}_2\text{O}_3-\text{CaO}-\text{MgO}-\text{Cr}_2\text{O}_3$  melts, and the structure of granulated samples with varying  $\text{FeO}/\text{SiO}_2$  ratios,  $\text{Al}_2\text{O}_3$  content, and  $\text{CaO}$  content was analyzed using Raman spectroscopy.  $\text{Cr}_2\text{O}_3$  was included in the system to more accurately reflect slag compositions encountered in the pyrometallurgical extraction of copper. Chromium comes into the process *via* electronic scrap and refractory dissolution and acts as a nucleation agent in the slag, promoting the formation of chromium-rich

spinel.<sup>[39,40]</sup> Solid phases influence the viscosity, which increases with the volume of solids.<sup>[41–43]</sup> Incorporating Cr<sub>2</sub>O<sub>3</sub> was therefore deemed essential for accurately reflecting the behavior of industrial slag viscosity.

The findings provide insights into the correlation between slag composition, ionic structure, and viscosity. These results have practical implications for improving industrial pyrometallurgical operations, particularly in optimizing slag handling and enhancing slag-cleaning processes, such as settling.

## II. EXPERIMENTAL

### A. Sample Composition and Synthesis

The influence of composition on viscosity and slag structure was estimated in a two-level full-factorial design of experiments with the three factors Al<sub>2</sub>O<sub>3</sub>, CaO content, and the FeO/SiO<sub>2</sub> ratio. The planned compositions, FeO/SiO<sub>2</sub> ratio, calculated liquidus temperature, and NBO/T are shown in Table I. The liquidus temperatures of the planned compositions were estimated using the Equilib module of FactSage 8.2<sup>[45]</sup> and the database GTOx. The calculations were performed in equilibrium with Fe crucibles and by disregarding the presence of a spinel phase (A(II)B(III)<sub>2</sub>O<sub>4</sub>). The samples in the experimental matrix are labeled as *L* or *H*, indicating whether the FeO/SiO<sub>2</sub> ratio was at the lower (*L*) or higher (*H*) level. For each numbered sample pair (e.g., 1L and 1H), the FeO/SiO<sub>2</sub> ratio varied while keeping all other factors constant.

Except for the samples in the experimental matrix, a triplicate sample was included, which was a center point for the Al<sub>2</sub>O<sub>3</sub> and CaO content and the FeO/SiO<sub>2</sub> ratio. However, the MgO content was higher than the remaining samples (6.80 at pct), disqualifying it from being a valid center point. The triplicate was synthesized and analyzed to verify the robustness of the viscosity measurements. The triplicate samples were analyzed in the rheometer at the beginning, middle, and end of the full-factorial design. In all samples in the experimental design, MgO and Cr<sub>2</sub>O<sub>3</sub> were included at a constant level of 1.50 and 0.08 at pct, respectively.

The samples were synthesized using the reagent-grade chemicals Fe, Fe<sub>2</sub>O<sub>3</sub>, SiO<sub>2</sub>, CaCO<sub>3</sub>, Al<sub>2</sub>O<sub>3</sub>, and Cr<sub>2</sub>O<sub>3</sub>. The dry chemicals were mixed, packed in Fe crucibles (>99.82 pct Fe), and melted in a Ruhstrat resistance-heated furnace under an inert atmosphere, using a gas mixture of N<sub>2</sub> (99.996 pct) and Ar (99.999 pct) with flow rates of 12 and 3 L/min, respectively. The Fe crucibles were used during the synthesis to provide an oxygen buffer to the system that would approach Fe–FeO conditions.<sup>[44]</sup>

The material was heated at a rate of 10 K/min until the temperature reached 100 K above the calculated liquidus temperature. The melt was held isothermally for one hour, removed manually from the furnace, and tapped into water jets with tap water (flow rate of 1.1 L/s). Andersson *et al.*<sup>[46]</sup> have published a more detailed description of the granulation procedure. The chemical composition of the samples was analyzed using a Philips PW2606 X-ray fluorescence (XRF) instrument (Malvern Panalytical, Malvern).

The analyzed chemical composition and FeO/SiO<sub>2</sub> ratio are shown in Table II. The analyzed FeO/SiO<sub>2</sub> ratios were higher than the target ratios of 1.08 and 1.25. This discrepancy may be due to iron dissolution from the crucible, matrix effects during XRF analysis, or a combination of both factors. The chemical analysis was used to assess the success of the synthesis.

### B. Viscosity Measurements

The viscosity measurements of the samples were performed using the rotating cylinder technique and a Mo spindle and crucible (tzm molybdenum 364). The rheometer system was an Anton Paar Furnace Rheometer System (FRS 1800) (Anton Paar GmbH, Austria). The temperature registered during the viscosity measurements was measured with a B-type thermocouple positioned in a hollow Al<sub>2</sub>O<sub>3</sub> shaft holding the crucible, approximately 5 mm from the bottom of the melt. Ar (99.999 pct purity) was introduced into the furnace *via* the crucible shaft, using a constant flow rate of 2.5 L/min during the entire experiment. A previous study comparing different crucible and spindle materials used for viscosity measurements showed that the Fe<sub>2</sub>O<sub>3</sub> content in slowly cooled samples increased from 4.1 to

**Table I. Planned Sample Composition, Calculated Liquidus Temperature (Temp.) Disregarding the Presence of a Spinel Phase and the FeO/SiO<sub>2</sub> Ratio, and NBO/T**

Sample	[K]	[At. Pct/At. Pct]	[At. Pct]						
	Liquidus Temp.	FeO/SiO <sub>2</sub>	SiO <sub>2</sub>	FeO	Al <sub>2</sub> O <sub>3</sub>	CaO	MgO	Cr <sub>2</sub> O <sub>3</sub>	NBO/T
1L	1486	1.08	45.99	49.83	1.40	1.20	1.50	0.08	2.10
2L	1395	1.08	44.27	47.95	5.00	1.20	1.50	0.08	1.68
3L	1401	1.08	40.81	44.21	1.40	12.00	1.50	0.08	2.58
4L	1366	1.08	39.08	42.34	5.00	12.00	1.50	0.08	2.07
1H	1443	1.25	42.59	53.23	1.40	1.20	1.50	0.08	2.40
2H	1409	1.25	40.99	51.23	5.00	1.20	1.50	0.08	1.92
3H	1411	1.25	37.79	47.23	1.40	12.00	1.50	0.08	2.92
4H	1368	1.25	36.19	45.23	5.00	12.00	1.50	0.08	2.33

5.9 wt pct in a  $\text{Fe}_1\text{O}-\text{SiO}_2-\text{Al}_2\text{O}_3$  system using a Mo crucible and spindle.<sup>[47]</sup> The viscosity measurements lasted approximately ten hours and used the same experimental setup as in this study.<sup>[47]</sup> This indicates that the oxidation of FeO to  $\text{Fe}_2\text{O}_3$  is limited in the experimental setup.

The measurements were started at the highest experimental temperature of 1723 K (1450°C). The viscosity was measured in a cooling cycle every 50 K from 1723 K to 1423 K. Before each viscosity measurement at a new temperature, the furnace was held at the target temperature for at least 45 min, while the spindle was rotated at a shear rate of  $4 \text{ s}^{-1}$  to ensure a homogeneous temperature in the melt. A constant viscosity at a fixed shear rate indicated that the melt had homogenized, taking up to 1 h for some of the compositions at a specific temperature. An automated program measured the viscosity with different constant shear rates of 1, 2, 4, 8, and  $16 \text{ s}^{-1}$ .

Notably, Mo was used as the spindle and crucible material during the viscosity measurements, resulting in the inevitable incorporation of Mo into the slag. Post-experimental analysis revealed that the Mo content in the samples ranged from 0.4 and 1.3 wt pct, with higher levels observed in samples containing a higher level of CaO. Given the relatively small percentage of Mo, its effect on viscosity is assumed to be minor.

### C. Raman Spectroscopy

A representative sample of each granulated melt was milled using a ring mill. X-ray diffraction (XRD) was used to estimate if the samples were amorphous before being analyzed with Raman spectroscopy. The XRD analysis was performed in a Malvern Panalytical Empyrean X-ray diffractometer (Malvern Panalytical, Malvern, U.K.) operating on copper  $K_\alpha$  generated at 45 kV and 40 mA. The scans were performed in the  $2\theta$  ranges of 10–90 deg with a step size of 0.0130 deg  $2\theta$  and a scan time of 698 s per step. The diffractograms were evaluated using HighScore + and the FIZ Karlsruhe inorganic crystal structure database.

The milled samples were then analyzed using Raman spectroscopy to determine the melt structure and the influence of FeO/SiO<sub>2</sub> ratio, Al<sub>2</sub>O<sub>3</sub>, and CaO. The Raman spectra of samples were collected in the 100–1200  $\text{cm}^{-1}$  spectral range by a confocal micro-Raman spectrometer from B&W Tek (Plainsboro, U.S.) with an excitation wavelength of 532 nm. The peak identification at specific wavenumbers, used for Gaussian deconvolution of Raman scattering data, was performed using the Peakfit software. The spectra were deconvolved by fitting the peaks corresponding to vibrations of various structural units, employing Gaussian line shapes.<sup>[48]</sup> Quantitative peak deconvolution was conducted over the Raman shift range from 400 to 1200  $\text{cm}^{-1}$ . The full widths of half maximum (FWHM) of various peaks were fixed to reduce the uncertainty of deconvolution.

## III. RESULTS AND DISCUSSION

### A. Viscosity

The repeatability of the experimental setup was evaluated by performing triplicate experiments labeled T1–T3. The viscosity of the samples is plotted as a function of temperature in Figure 1. The results demonstrate good repeatability, with the standard deviation not exceeding 3 pct of the average viscosity across the triplicate measurements. Notably, the viscosity data from the first and last experiments (T1 and T3) were nearly identical. The standard deviation reflects the combined error associated with synthesizing the samples and conducting the viscosity measurements, as each triplicate involved independently synthesized samples.

The viscosity measurements of all samples in the experimental design across the entire temperature range are shown in Figure 2. Overall, the viscosity increased for each composition as the temperature decreased. At higher temperatures, the increased kinetic energy in the melt enhances the random motions of atoms and molecules, facilitating particle migration and resulting in lower viscosity.

As shown in Figure 2, the slopes of the viscosity-temperature data were steeper at lower temperatures. For example, in sample 1L (FeO/SiO<sub>2</sub>=1.08, CaO=1.2 at pct, Al<sub>2</sub>O<sub>3</sub>=1.4 at pct), the slope becomes noticeably steeper below 1573 K (highlighted with a circle in Figure 2). This behavior is attributed to the formation of solids in the melt when the temperature is below the liquidus temperature, leading to an increased viscosity. The formation of precipitated solids was further indicated during the homogenization at new temperatures during the viscosity measurements, as the viscosity increased over time under a constant shear rate, necessitating extended homogenization periods.

The sample with all factors at the lower level, 1L, initially exhibited a lower viscosity than sample 2L (Al<sub>2</sub>O<sub>3</sub>=5.0 at pct). However, below 1573 K, the viscosity of sample 1L increased due to the formation of solids, reaching values comparable to those of sample 2L, which had a higher Al<sub>2</sub>O<sub>3</sub> content.

When the samples were fully liquid, the highest viscosity was measured in sample 2L, with a FeO/SiO<sub>2</sub> ratio of 1.08, low CaO, and high Al<sub>2</sub>O<sub>3</sub> content. In contrast, the lowest viscosity was recorded for sample 3H, which had a FeO/SiO<sub>2</sub> ratio of 1.25, high CaO content, and low Al<sub>2</sub>O<sub>3</sub> content. The most significant viscosity difference was observed between these two opposing compositions. At 1573 K, the viscosity of sample 3H was 0.10 Pa s, while it was 0.35 Pa s for sample 2L, 3.5 times higher than that of sample 3H.

Table I shows the calculated ratio of the non-bridging oxygen per tetrahedron (NBO/T) ratio<sup>[49]</sup> based on the planned composition shown in Table I. The NBO/T for the samples ranges from 1.68 to 2.92. When correlating the NBO/T to the viscosity, it can be seen that the viscosity generally decreases with increasing NBO/T of the samples, indicating that more depolymerized slags have a lower viscosity. For example, the sample with the

**Table II. Analyzed Chemical Composition and FeO/SiO<sub>2</sub> Ratio**

Sample	[At. Pct/At. Pct]			[At. Pct]			
	FeO/SiO <sub>2</sub>	SiO <sub>2</sub>	FeO	Al <sub>2</sub> O <sub>3</sub>	CaO	MgO	Cr <sub>2</sub> O <sub>3</sub>
1L	1.2	43.9	51.2	2.0	1.3	1.5	0.1
2L	1.3	40.7	51.1	5.0	1.3	1.7	0.1
3L	1.1	39.4	44.8	2.0	12.0	1.6	0.1
4L	1.2	37.0	44.3	4.9	12.1	1.7	0.1
1H	1.4	40.2	54.9	2.0	1.3	1.5	0.1
2H	1.4	38.6	53.4	4.9	1.3	1.7	0.1
3H	1.3	36.7	47.8	1.9	12.0	1.5	0.1
4H	1.3	35.1	46.3	4.8	12.0	1.7	0.1

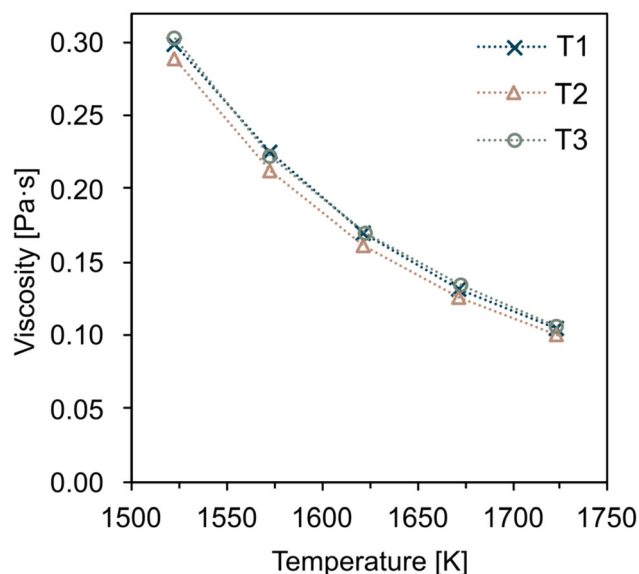


Fig. 1—Viscosity data of the triplicate in the temperature interval from 1523 K to 1723 K.

highest viscosity has the lowest NBO/T of 1.68 and the sample with the lowest viscosity has the highest NBO/T of 2.92.

The viscosity data were plotted over the temperature range from 1573 K to 1723 K, where all samples appeared fully liquid, as shown in Figures 3(a) and (b). Figure 3(a) shows the viscosity data for samples with a low FeO/SiO<sub>2</sub> ratio (labeled 1L–4L), while Figure 3(b) shows the viscosity of samples with a high FeO/SiO<sub>2</sub> ratio (labeled 1H–4H).

Evaluating the compositional factors individually, it was concluded that CaO had the most significant impact on viscosity in the given intervals, followed by the FeO/SiO<sub>2</sub> ratio, which both contributed to a lower viscosity. The effect of CaO was more pronounced at the lower FeO/SiO<sub>2</sub> ratio (Figure 3(a)), as evidenced by comparing the difference between the data series with the same color in the figures. This can be attributed to the higher number of Si–O–Si bonds in more polymerized melts (lower FeO/SiO<sub>2</sub> ratio), broken by the basic oxides like CaO. At higher FeO/SiO<sub>2</sub> ratios, both FeO and CaO act as network breakers, potentially producing excess free oxygen (O<sup>2-</sup>). No amphoteric behavior related to FeO

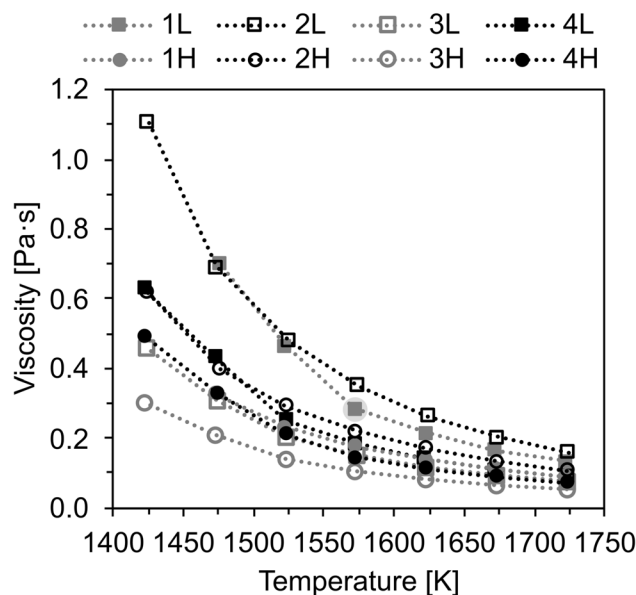


Fig. 2—The viscosity data over the entire temperature interval (1423 K–1723 K). The samples marked with L have the lower FeO/SiO<sub>2</sub> ratio (1.08 at. pct/at. pct), and those marked with H have the higher (1.25 at. pct/at. pct).

content was observed in the compositional ranges in the current study. However, the Fe<sup>3+</sup> content was not analyzed in the samples. Pargamin *et al.*<sup>[50]</sup> studied the repartition of Fe atoms between Fe<sup>2+</sup> and Fe<sup>3+</sup> and the distribution of Fe<sup>3+</sup> among octahedral and tetrahedral sites in a CaO–SiO<sub>2</sub>–Fe<sub>2</sub>O<sub>3</sub> system. The samples were equilibrated in air at 1550°C before being quenched. The content of Fe<sup>2+</sup> and Fe<sup>3+</sup> and the distribution of Fe<sup>3+</sup> among octahedral and tetrahedral sites were analyzed using Mössbauer spectroscopy. The results showed that the ratio of tetrahedral coordinated Fe<sup>3+</sup> over the sum of tetrahedral and octahedral Fe<sup>3+</sup> remained approximately unchanged at around 0.3 when the Fe<sub>2</sub>O<sub>3</sub> content increased in the series when the basicity (wt pct CaO/wt pct SiO<sub>2</sub>) was around 0.54.<sup>[50]</sup> This means most of the Fe<sup>3+</sup> was octahedrally coordinated, acting as network modifiers. However, the basicity of this study was higher than that of the present. Moreover, the Fe<sup>3+</sup> content is assumed to be lower in the present study as the melts were synthesized in Fe crucibles in an inert

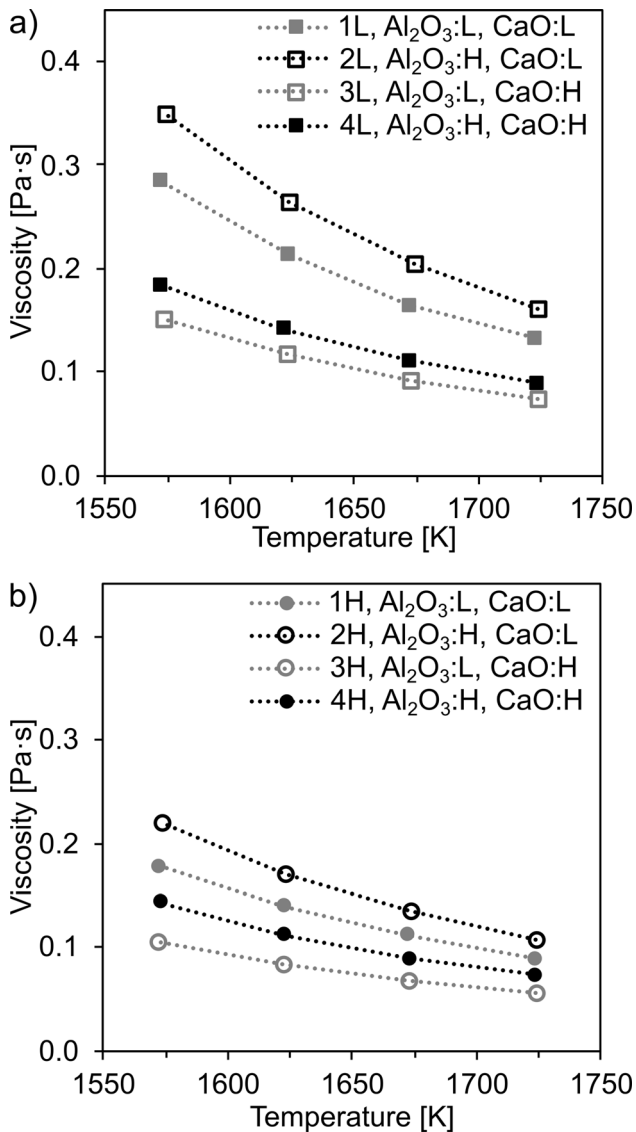


Fig. 3—The viscosity data in the temperature range from 1573 K to 1723 K. The samples marked with L have the lower FeO/SiO<sub>2</sub> ratio (1.08 at. pct/at. pct), and those marked with H have the higher (1.25 at. pct/at. pct). Al<sub>2</sub>O<sub>3</sub>:L equals a content of 1.4 at. pct, and Al<sub>2</sub>O<sub>3</sub>:H equals 5.0 at. pct. CaO:L equals 1.2 at. pct, and CaO:H equals 12 at. pct.

atmosphere. At the higher FeO/SiO<sub>2</sub> ratio (1.25 wt pct/wt pct), the Fe<sup>3+</sup> content was expected to increase. The viscosity measurements show that the viscosity decreased with the increasing ratio; thus, most of the Fe<sup>3+</sup> was expected to be octahedrally coordinated. However, this factor must be isolated and further studied to be verified in the relevant melt system.

Silicate-containing melts have a disordered three-dimensional network of silicate tetrahedra in the form of irregular rings and chains. These structures can deform through the random motion of atoms and molecules. However, the covalent bonds between the silicon and oxygen atoms resist deformation, resulting in higher viscosity in melts with high silica content. Adding network-breaking oxides like CaO and FeO can disrupt

the bridging oxygen between the silicon atoms, resulting in non-bridging oxygen and, thus, a more depolymerized melt with a lower viscosity.

Previous studies have consistently demonstrated that adding CaO reduces viscosity,<sup>[32–37]</sup> which supports this study's findings. From an industrial perspective, achieving a slag with low viscosity is advantageous. According to this study, this can be accomplished by operating with lower SiO<sub>2</sub> additions to obtain a higher FeO/SiO<sub>2</sub> ratio and modifying the slag with CaO.

In contrast, the higher level of Al<sub>2</sub>O<sub>3</sub> (5 at. pct) increased the viscosity in all samples. From Figures 3(a) and (b), it can be seen that the effect of Al<sub>2</sub>O<sub>3</sub> on the viscosity was most pronounced when comparing the viscosity data from samples 1L and 2L, as the absolute difference of the viscosity between these samples is largest, keeping all other parameter constants. The explanation is that Al<sub>2</sub>O<sub>3</sub> can act as a network-forming oxide in the melt, meaning the increased Al<sub>2</sub>O<sub>3</sub> content increases the viscosity. When Al<sub>2</sub>O<sub>3</sub> acts as a network-forming oxide, it forms a tetrahedron ([AlO<sub>4</sub>]<sup>−5</sup>), incorporating the silicate network-forming Si–O–Al bonds. These findings align with the study by Mostaghel *et al.*,<sup>[26]</sup> which investigated the impact of Al<sub>2</sub>O<sub>3</sub> additions on viscosity in an industrial iron silicate slag with a FeO/SiO<sub>2</sub> ratio similar to the lower one in this study (1.08 at. pct/at. pct). The results also align with the study by Wang *et al.*,<sup>[24]</sup> studying the effect of Al<sub>2</sub>O<sub>3</sub> on viscosity in systems with similar FeO/SiO<sub>2</sub> ratios as the lower level in this study but had constant CaO and MgO contents of 8 wt pct and 3 wt pct, respectively. The results showed an increase in viscosity corresponding to higher Al<sub>2</sub>O<sub>3</sub> content.<sup>[24]</sup>

The compositional effect on viscosity was further evaluated by comparing the relationship between the molar ratio (at. pct/at. pct) of (Al<sub>2</sub>O<sub>3</sub> + SiO<sub>2</sub>)/MO (where MO is the basic oxides CaO, MgO, and FeO) and the viscosity at 1723 K, shown in Figure 4(a). The calculated ratio was separately based on the planned and analyzed melt composition. Figure 4(a) shows a linear relationship between the (Al<sub>2</sub>O<sub>3</sub> + SiO<sub>2</sub>)/MO ratio and viscosity, with *R*<sup>2</sup> values of 0.92 and 0.97 for the analyzed and planned compositions, respectively. The main difference between the planned and analyzed compositions is the FeO/SiO<sub>2</sub> ratio, which was higher than expected in the analyzed samples. This discrepancy may be due to matrix effects during XRF analysis. Based on the XRF analysis, the FeO/SiO<sub>2</sub> ratio of 2L (the sample with the highest viscosity) was higher than expected, which decreases the calculated ratio, resulting in a deviation from the linear trend. However, a good linear fit (*R*<sup>2</sup> = 0.97) is obtained between the planned composition and the viscosity, indicating that Al<sub>2</sub>O<sub>3</sub> and SiO<sub>2</sub> act as network-forming oxides in the melts, polymerizing the melt and, thus, increasing the viscosity.

Additionally, the effect of Al<sub>2</sub>O<sub>3</sub> on viscosity was compared by calculating the ratio of the viscosity (*η*) for samples with higher and lower Al<sub>2</sub>O<sub>3</sub> content ( $\frac{\eta_{Al_2O_3:H}}{\eta_{Al_2O_3:L}}$ ), shown in Figure 4(b). When comparing the viscosity ratio over the temperature range from 1723 K to 1523 K in Figure 4(b), it was observed that viscosity increased

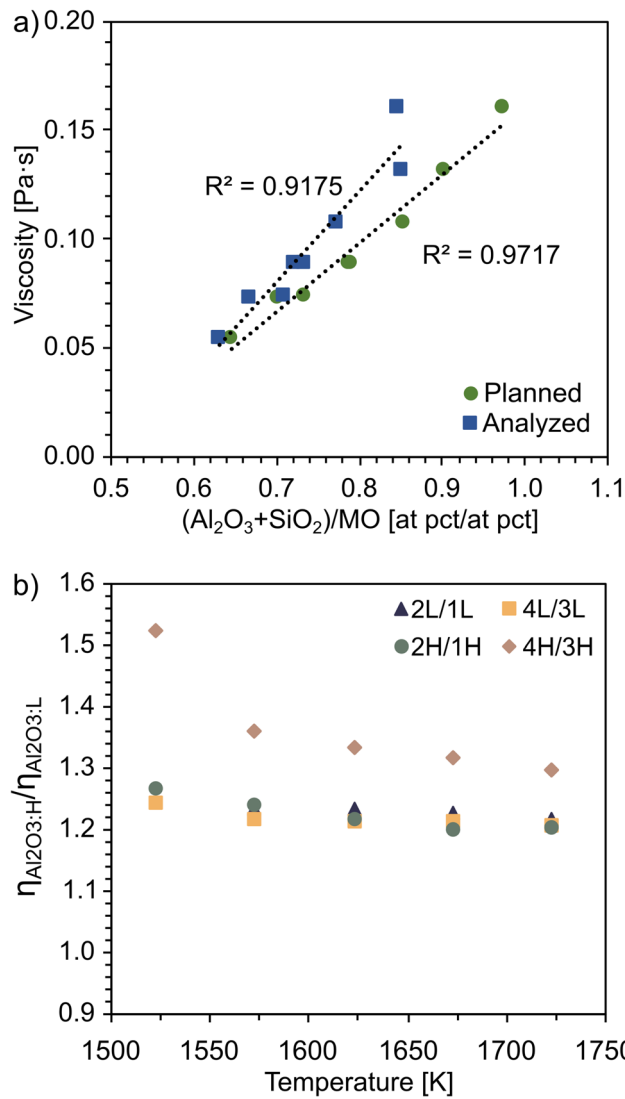


Fig. 4—(a) The correlation between  $(\text{Al}_2\text{O}_3 + \text{SiO}_2)/\text{MO}$  and viscosity at 1723 K and (b) the ratio of viscosities for samples with higher and lower  $\text{Al}_2\text{O}_3$  content.

by 21 to 22 pct at 1723 K when the  $\text{Al}_2\text{O}_3$  content was higher, with all other factors kept constant. However, for the ratio of 4H over 3H, the increase in viscosity was more pronounced, reaching 32 pct at 1723 K and increased as the temperature decreased. The highest ratio at 1523 K is explained by solids formed in 4H, significantly increasing the viscosity.

Park *et al.*<sup>[19]</sup> demonstrated the amphoteric behavior of  $\text{Al}_2\text{O}_3$  while examining the influence of  $\text{Al}_2\text{O}_3$  content (at a fixed  $\text{Fe}/\text{SiO}_2$  ratio) on viscosity in a  $\text{FeO}_t\text{-Al}_2\text{O}_3\text{-SiO}_2$  system. The results indicated an initial decrease in viscosity with increasing  $\text{Al}_2\text{O}_3$ , reaching a minimum before increasing at higher  $\text{Al}_2\text{O}_3$  concentrations. This behavior was attributed to the amphoteric behavior of  $\text{Al}_2\text{O}_3$ , wherein it initially acts as a basic oxide and shifts to an acidic oxide as slag composition changes.<sup>[19]</sup>

The amphoteric behavior of  $\text{Al}_2\text{O}_3$  is related to the coordination of  $\text{Al}^{3+}$  in an octahedral or tetrahedral structure.<sup>[29,30]</sup> McMillan *et al.*<sup>[51,52]</sup> and Poe *et al.*<sup>[53,54]</sup> presented that the coordination number of  $\text{Al}^{3+}$  is

correlated to the  $\text{Ca}/\text{Al}$  ratio in a  $\text{CaO-Al}_2\text{O}_3$  system because of the role of  $\text{Ca}^{2+}$  as a charge compensator to the tetrahedrally coordinated aluminum ( $[\text{AlO}_4]^{-5}$ ). In the current study, no amphoteric behavior of  $\text{Al}_2\text{O}_3$  could be distinguished; however, it acts as a more vigorous acid when the melts are more depolymerized. This can be explained by the charge compensator effect of the basic oxides  $\text{Ca}^{2+}$ , making it possible for  $\text{Al}_2\text{O}_3$  to form  $\text{AlO}_4$ -tetrahedrons to a more significant extent in the melt. However, this cannot be verified with only two levels of  $\text{Al}_2\text{O}_3$ , as in this study.

### B. Activation Energy of Flow

The viscosity of liquids is well known to decrease with increasing temperature.<sup>[16,55,56]</sup> The temperature dependence of the viscosity for a given melt composition can be described by an Arrhenius-type relationship,<sup>[57]</sup> shown in Eq. [1].

$$\eta = A \exp\left(\frac{E_a}{RT}\right), \quad [1]$$

where  $\eta$  is the viscosity in Pa s,  $A$  is the pre-exponential factor (Pa s),  $E_a$  is the activation energy of flow in J/mol,  $T$  is the absolute temperature in K, and  $R$  is the gas constant (8.341 J/mol K). If the melt follows this relationship, the natural logarithm of the viscosity ( $\ln(\eta)$ ) versus the reciprocal of temperature gives a linear relationship, and the slope of the line reflects the activation energy.

The activation energy for viscous flow is considered to be the energy required to break the bonds necessary for movement. Consequently, it reflects the effect of structure on physical properties.<sup>[13,18]</sup> A linear relationship of the measured data indicates that the material has been fully liquid and that the melt follows an Arrhenius behavior. Deviations from a linear system may be due to precipitated solids in the melt. Roscoe developed a well-known model based on Einstein's approach, the Einstein-Roscoe equation, which describes the viscosity of melts with solid particles,<sup>[41,42,58]</sup> showing that the melt viscosity increases when solids are present. Additionally, the melt composition changes when solids form, affecting the viscosity.

$\ln(\eta)$  was plotted against  $1/T$  in the temperature range where the samples remained liquid, resulting in  $R^2$  values between 0.9980 and 0.9999. The liquidus area was estimated by determining where the data deviated from a linear fit.<sup>[52]</sup> The values for the activation energy highlight the structural changes with temperature. Table III presents the samples' activation energy and pre-exponential factor.

The activation energy plotted against the  $\text{NBO}/T$  is shown in Figure 5(a). In general, it is shown that the activation energy decreases with increasing  $\text{NBO}/T$  in both series with different  $\text{FeO}/\text{SiO}_2$  ratios. The sample with the highest activation energy was 2L, and the sample with the lowest was 3H. Notably, these samples had the highest and lowest viscosity at all temperatures and the lowest and highest  $\text{NBO}/T$ , respectively, suggesting that more polymerized slags are more sensitive to temperature changes.

**Table III. Activation Energy, Material Constant,  $R^2$  Value**

Sample	Activation Energy, $E_a$ [kJ/mol] (Temperature Range $\pm$ 3 K)	Pre-exponential Factor, A [ $10^{-5}$ Pa s]	$R^2$
1L	115.8 (1723–1573)	4.01	0.9990
2L	123.0 (1723–1473)	2.26	0.9992
3L	110.5 (1723–1523)	3.27	0.9991
4L	112.8 (1723–1523)	3.35	0.9982
1H	104.3 (1723–1523)	6.13	0.9999
2H	111.7 (1723–1473)	4.37	0.9992
3H	100.7 (1723–1473)	4.77	0.9980
4H	101.3 (1723–1573)	6.15	0.9994

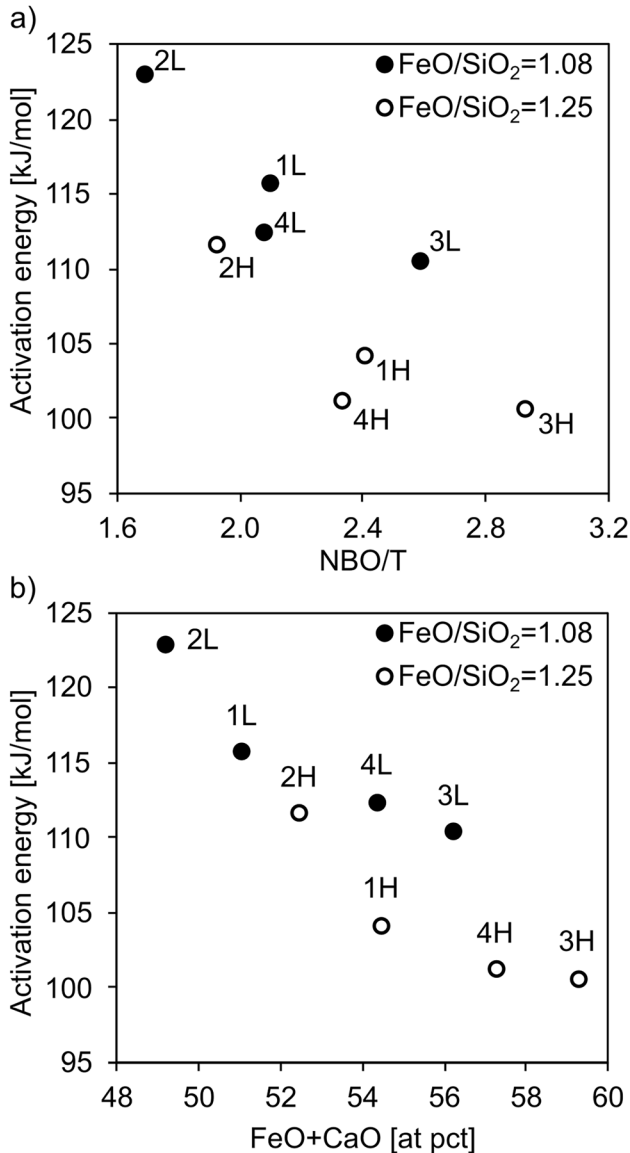


Fig. 5—Activation energy plotted against the (a) NBO/T and (b) FeO and CaO content.

When evaluating the activation energy and the effect of individual parameters, it can be seen that the samples with a FeO/SiO<sub>2</sub> ratio of 1.25 had lower activation energy than the samples with the same composition but a FeO/SiO<sub>2</sub> ratio of 1.08, the same trend was seen for the

CaO content where those with a high CaO content (12 at pct) had lower activation energy. This indicates that a higher FeO/SiO<sub>2</sub> ratio and CaO content decrease the energy barrier for viscous flow by depolymerizing the melt. As shown by Choi *et al.*<sup>[59]</sup> the activation energy decreases when the FeO content increases due to a change in the flow unit, which goes from Si–O–Si to Fe–O–Si and Fe–O–Fe. The activation energy calculated by Wang *et al.*<sup>[20]</sup> in a FeO–Fe<sub>2</sub>O<sub>3</sub>–SiO<sub>2</sub>–8 wt pct CaO–3 wt pct MgO–3 wt pct Al<sub>2</sub>O<sub>3</sub> system with varying Fe/SiO<sub>2</sub> ratios (wt pct/wt pct) of 0.8, 1.0, and 1.2 decreased with increasing Fe/SiO<sub>2</sub> ratio. The activation energy of the sample with a Fe/SiO<sub>2</sub> ratio of 1.2 and a Fe<sub>2</sub>O<sub>3</sub> content of 4 wt pct equaled 112.4 kJ/mol,<sup>[20]</sup> comparable with sample 1H in this study.

Earlier studies by Choi *et al.*<sup>[60]</sup> have shown that the activation energy decreases with increasing Fe<sub>1</sub>O content before reaching a constant value in a CaO–SiO<sub>2</sub>–Fe<sub>1</sub>O–10 wt pct Al<sub>2</sub>O<sub>3</sub>–10 wt pct MgO–10 wt pct MnO with basicities (wt pct CaO/wt pct SiO<sub>2</sub>) between 0.6 and 0.8. The dependency of Fe<sub>1</sub>O on the activation energy was suggested to be due to a change in the viscous flow unit according to the primary phase that changed from melilite, olivine, spinel, and monoxide at the highest Fe<sub>1</sub>O contents.<sup>[60]</sup>

For the present study, the basicity was at its highest, close to 0.3 for the samples with a higher CaO content and near 0.03 for those with a lower. According to the FactSage calculations, the primary phase crystallized was cristobalite for 1L, a spinel phase for 2L and 2H, and olivine for the remaining samples. The diffractograms in Figure 6 indicate the presence of cristobalite (SiO<sub>2</sub>) in 1L and 2H, wüstite (FeO) in 4L, and a spinel phase in 3H and 4H. However, only a few peaks were identified, indicating the samples were nearly amorphous.

Figure 5(b) shows the activation energy as a function of the FeO and CaO content in the planned composition shown in Table I. The figure shows that the activation energy decreases when the content of FeO and CaO increases, with a shift to lower activation energies when the FeO/SiO<sub>2</sub> ratio is higher. Adding the basic oxides FeO and CaO to the slag decreased the activation energy and, thus, temperature dependence, as Fe and Ca gradually change the amount of Si–O–Si and Si–O–Al bonds to Fe(Ca)–O–Si (olivine) and Fe–O–Fe(Al) (spinel phase) and possibly to Fe–O bonds (monoxide) for 4L. When the FeO + CaO content reaches above 57 at pct, the activation energy is indicated to reach a constant value. However, this needs to be studied

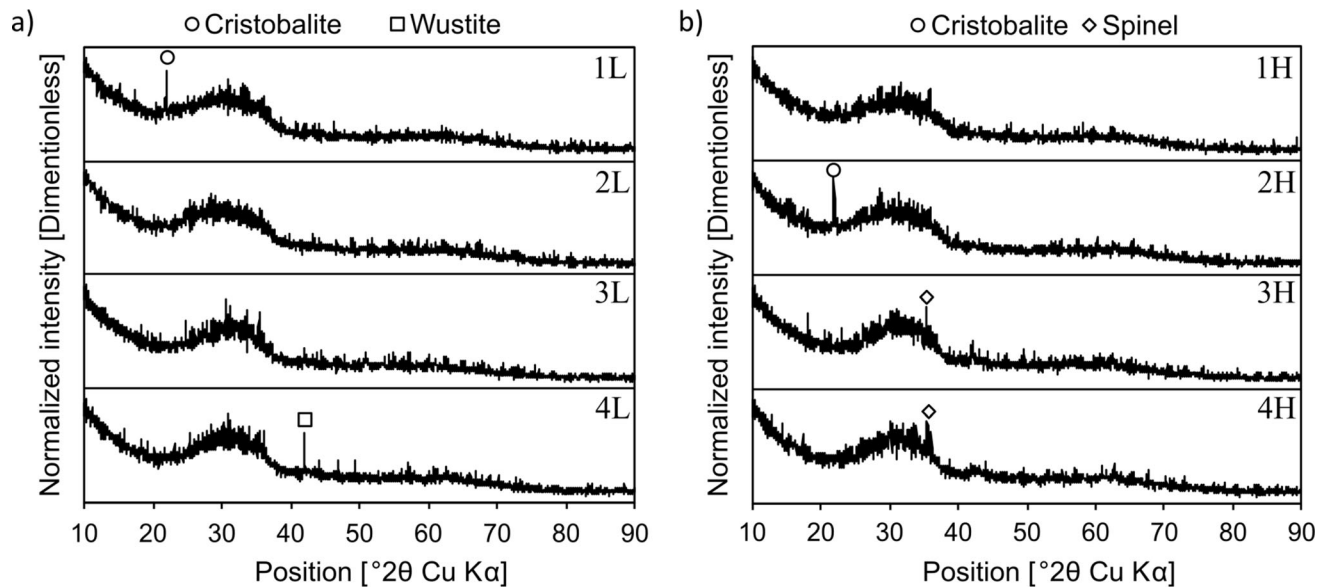


Fig. 6—Diffractograms of the water-granulated samples (a) 1L–4L and (b) 1H–4H.

further, including additional compositions. The effect of CaO, decreasing the activation energy, was more significant when the FeO/SiO<sub>2</sub> ratio was lower, meaning that the CaO is a more efficient network breaker when the slag is more polymerized. Regarding the FeO/SiO<sub>2</sub> ratio and the CaO content, the FeO/SiO<sub>2</sub> ratio has a more prominent effect on the activation energy in the given intervals.

Opposite to this, the higher Al<sub>2</sub>O<sub>3</sub> content (5 at pct) increased the activation energy. These results reflect the correlation between the activation energy and the structure of the melt, where a melt with a higher polymerization degree (NBO/T) is more sensitive to temperature changes. The effect of Al<sub>2</sub>O<sub>3</sub> is in accordance with the study by Wang *et al.*<sup>[24]</sup>; however, the activation energy calculated in that study was higher, ranging from 119.45 to 155.30 kJ/mol (0–12 wt pct Al<sub>2</sub>O<sub>3</sub>), which can be explained by the wider temperature range down to 1400 K. Additionally, the study suggested that the melts became more polymerized with an increasing Al<sub>2</sub>O<sub>3</sub> content.<sup>[24]</sup>

The effect of Al<sub>2</sub>O<sub>3</sub>, increasing the activation energy, is higher when the CaO content is lower. This can be seen by comparing, *e.g.*, 1L and 2L with 3L and 4L, where 1L and 2L have a lower CaO content and 2L and 4L have a higher Al<sub>2</sub>O<sub>3</sub> content. In both FeO/SiO<sub>2</sub> series, the effect of Al<sub>2</sub>O<sub>3</sub> on activation energy is more pronounced when the CaO content is lower. This is strengthened by evaluating the three samples, 3L, 4L, and 2H, with a similar activation energy of 110.5, 112.8, and 111.7, respectively. Samples 3L and 4L have a higher level of CaO and lower FeO/SiO<sub>2</sub> ratio; the difference in composition is the Al<sub>2</sub>O<sub>3</sub> content, implying that a more depolymerized melt is less sensitive to Al<sub>2</sub>O<sub>3</sub> additions, referring to activation energy. Sample 2H has a high ratio of FeO/SiO<sub>2</sub>, depolymerizing the melt, and a higher level of Al<sub>2</sub>O<sub>3</sub>, polymerizing the melt and

increasing the activation energy. Thermal heat breaks the bond between the Si–O–Si, decreasing viscosity when temperature increases. Al<sub>2</sub>O<sub>3</sub> can absorb O<sup>2-</sup> in the melt to form a tetrahedral structure, [AlO<sub>4</sub>]<sup>5-</sup>, embedded in the silicate network structure, forming Si–O–Al bonds, resulting in a more viscous polymerized melt, making it more sensitive to temperature changes.

### C. Raman Spectroscopy

The diffractograms of the milled water-granulated samples are presented in Figure 6. The XRD analysis confirmed that the materials were predominantly amorphous. However, in samples 1L and 2H, a peak corresponding to cristobalite was detected, and in sample 4L, peaks corresponding to wüstite were detected. Sample 1L was the sample with the highest calculated liquidus temperature of 1486 K, meaning the granulation temperature was 1586 K. According to the viscosity measurements, the lowest temperature that still followed the Arrhenius relationship was 1573 K, which was relatively close to the granulation temperature, meaning that the cristobalite particles could have precipitated during the granulation and cooling of the samples. Peaks could also be present in sample 3L. However, it was inconclusive to determine if there were peaks or noise from the measurement.

In samples 3H and 4H, peaks corresponding to spinel were detected. Ion migration is related to energy barriers to crystallization.<sup>[61]</sup> The viscosities of the melts indirectly assess the differences in the degree of polymerization and ion mobility, whereas melts with lower viscosity have higher ion mobility. 3H and 4H were the samples with the lowest measured viscosity at all temperatures. This could explain why a crystalline phase was detected in these samples after water granulation, even if the experimental temperature before granulation was above the calculated liquidus temperature.

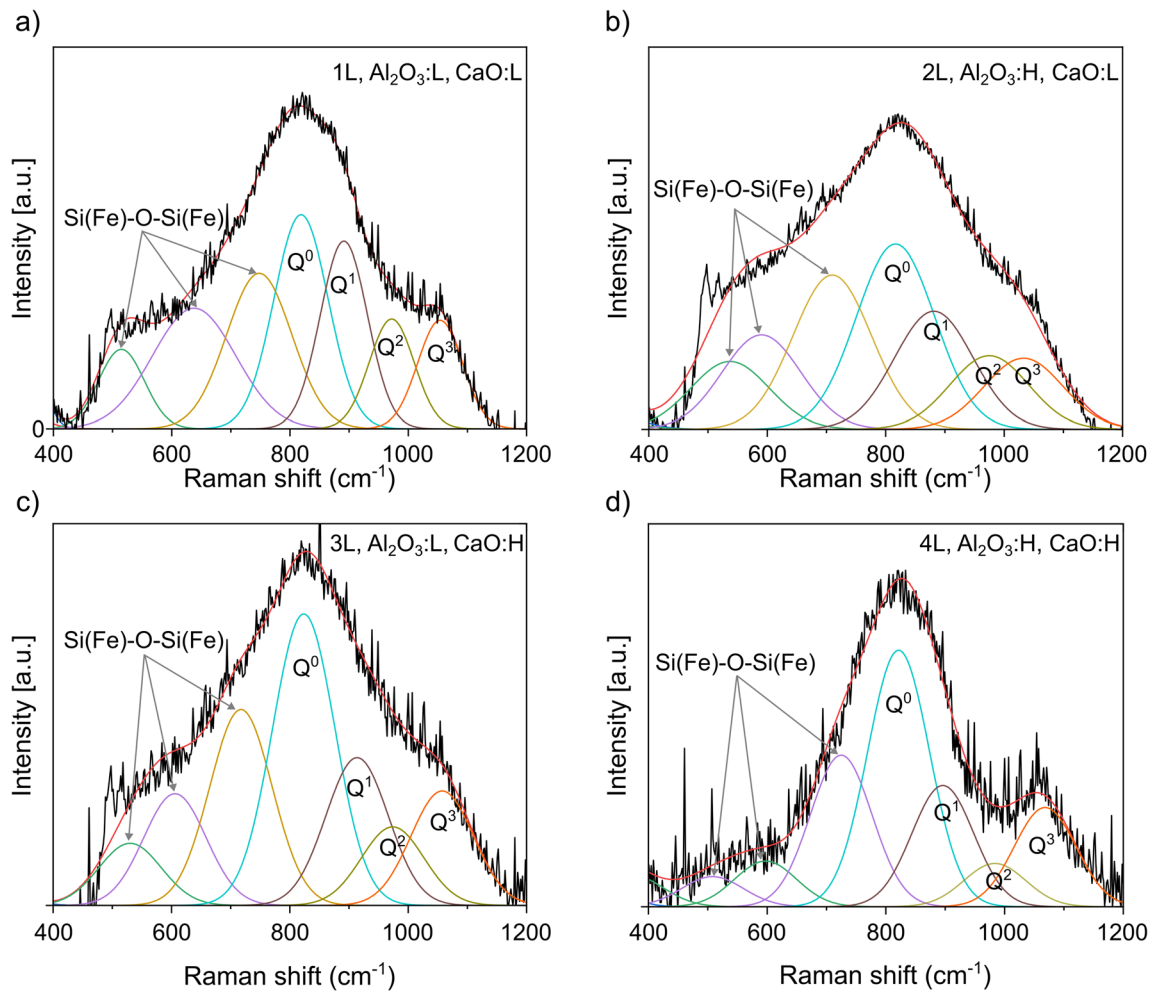


Fig. 7—Deconvoluted Raman spectra of samples with a low FeO/SiO<sub>2</sub> ratio (1.08), showing: (a) 1L—all factors low levels, (b) 2L—low CaO and high Al<sub>2</sub>O<sub>3</sub>, (c) 3L—high CaO and low Al<sub>2</sub>O<sub>3</sub>, and (d) 4H—high CaO and Al<sub>2</sub>O<sub>3</sub> high.

The Raman spectra were analyzed to characterize the water-granulated structure of the samples. Sharp peaks were found in the Raman spectra, possibly due to the residue crystalline phases in the water-granulated samples. The collected Raman spectra had envelopes in the medium frequency range (400–800 cm<sup>-1</sup>) and high frequency (800–1200 cm<sup>-1</sup>).

The Raman bands within medium frequency correspond to the bending vibration of the oxygen bridge Si(Fe)–O–Si(Fe). Iron is a multivalent element, which can have different coordination numbers in glass depending on the composition, atmosphere, and temperature.<sup>[62]</sup> Since FeO is the main iron species, as expected from the sample preparation, it is considered that the quantity of 4-coordinated iron (tetrahedral) existing in the glass structure is limited and that FeO mainly acts as a network-breaking oxide (6-coordinated structure),<sup>[63]</sup> which also was indicated by the viscosity measurements. The Si–O–Si oxygen bridge could be dominant. However, the medium-frequency bands could also represent Al–O–Si oxygen bridging for samples with higher alumina content.

The high-frequency Raman bands represent the stretching vibration of various silicate structural units with the number of bridging oxygens from 0 to 3. The high-frequency envelopes were deconvoluted into individual bands by assuming a Gaussian line shape. This study adopts Q<sup>n</sup> to represent the structural unit of the symmetric stretching band of ([SiO<sub>4</sub>]<sup>4-</sup>) tetrahedra, where n represents the number of bridging oxygen in the tetrahedra. Q<sup>n</sup> is generally available in the silicate structure as monomer silicate units (Q<sup>0</sup>), dimer silicate units (Q<sup>1</sup>), chain-like silicate structures (Q<sup>2</sup>), and sheet-like silicate structures (Q<sup>3</sup>). It should be mentioned that Al and Fe could also be incorporated into the silicate network if they exist in tetrahedral coordination.<sup>[63]</sup> The Q<sup>n</sup>s presented here are considered structural units with 4-coordinated Si, Al, and Fe at the center.

The high-frequency envelope can be deconvoluted by the bands from stretching vibrations of Q<sup>0</sup> (monomers) with a Raman shift of 810–830 cm<sup>-1</sup> [48,64–66], Q<sup>1</sup> (dimers) with a Raman shift 880–910 cm<sup>-1</sup>, Q<sup>2</sup> (chains) with a Raman Shift 970–990 cm<sup>-1</sup>, and Q<sup>3</sup> (rings) with a Raman shift 1030–1060 cm<sup>-1</sup> [48,64–71].

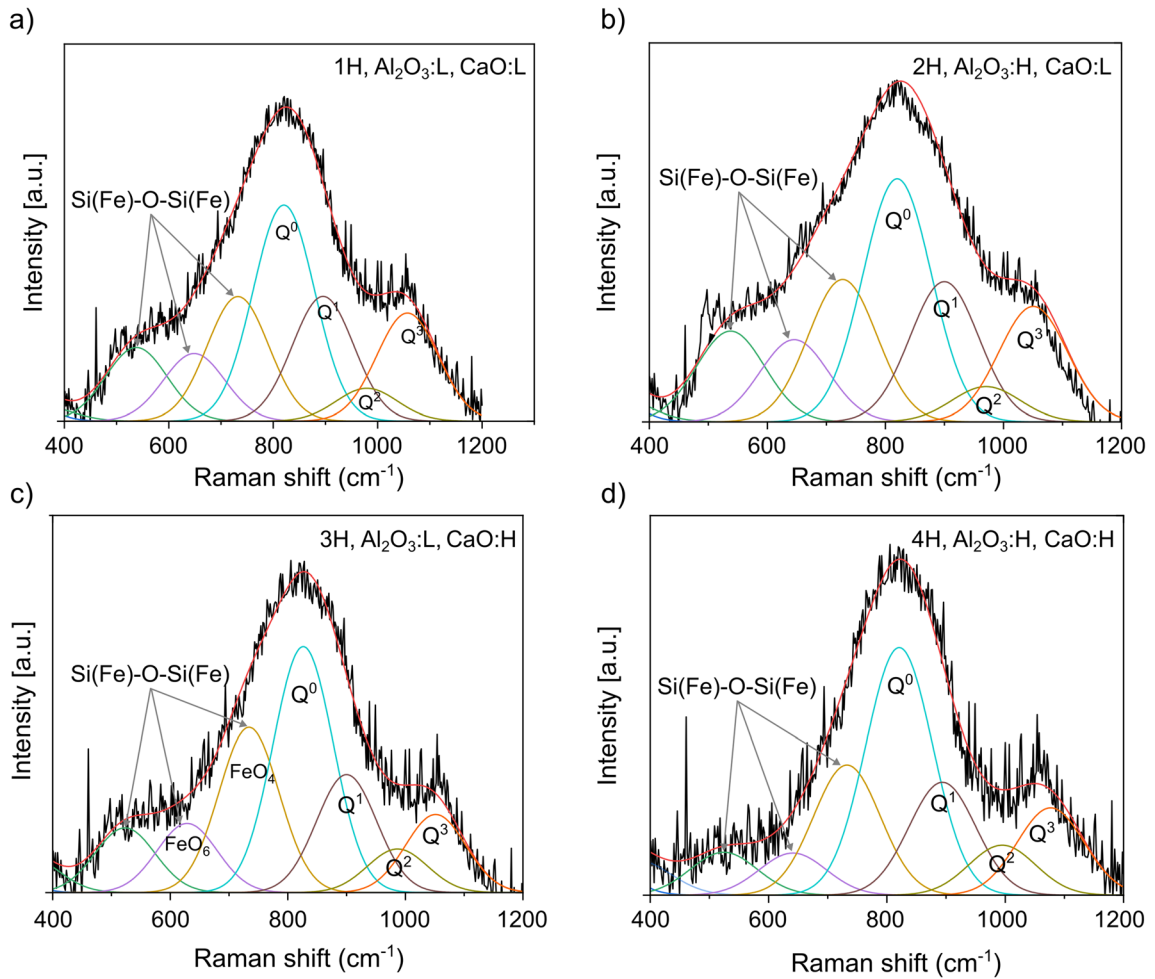


Fig. 8—Deconvoluted Raman spectra of samples with a high FeO/SiO<sub>2</sub> ratio (1.25), showing: (a) 1L—all factors low levels, (b) 2L—low CaO and high Al<sub>2</sub>O<sub>3</sub>, (c) 3L—high CaO and low Al<sub>2</sub>O<sub>3</sub>, and (d) 4H—high CaO and Al<sub>2</sub>O<sub>3</sub> high.

**Table IV. Relative Area Fractions of Q<sup>0</sup>, Q<sup>1</sup>, Q<sup>2</sup>, and Q<sup>3</sup> that Were Obtained from the Deconvoluted Raman Spectra and the Calculated Q<sup>0</sup>/Q<sup>1</sup> Ratios**

Sample	Relative Area Fractions				Q <sup>0</sup> /Q <sup>1</sup>
	Q <sup>0</sup>	Q <sup>1</sup>	Q <sup>2</sup>	Q <sup>3</sup>	
1L	0.42	0.29	0.13	0.16	1.44
2L	0.42	0.28	0.14	0.16	1.48
3L	0.46	0.23	0.12	0.18	1.97
4L	0.49	0.23	0.08	0.19	2.11
1H	0.43	0.27	0.13	0.17	1.61
2H	0.43	0.26	0.15	0.16	1.64
3H	0.51	0.24	0.09	0.16	2.08
4H	0.50	0.23	0.10	0.18	2.19

The deconvolution results of samples 1L–4L are shown in Figures 7(a)–(d), and the deconvolution results of 1H–4H are shown in Figures 8(a)–(d). The integrated area of Q<sup>n</sup> peaks can be used to calculate the number of structural units in the samples. The areas of individual peaks were calculated from the deconvolution plots, and

the relative area fractions of Q<sup>0</sup>, Q<sup>1</sup>, Q<sup>2</sup>, and Q<sup>3</sup> are shown in Table IV. Q<sup>0</sup> and Q<sup>1</sup> are the most abundant structural units in the samples, which means that the silicate network in the melt structure of the samples was largely depolymerized and mainly consisted of monomer silicate units ([SiO<sub>4</sub>]<sup>4-</sup>) and dimer silicate units ([Si<sub>2</sub>O<sub>7</sub>]<sup>6-</sup>). Melts dominated by Q<sup>0</sup> and Q<sup>1</sup> have a lower viscosity than those dominated by more polymerized structures, such as Q<sup>2</sup> and Q<sup>3</sup>, meaning they contain smaller structural units directly linked to the viscosity.

Q<sup>0</sup>/Q<sup>1</sup> ratios for various samples illustrate the variation of depolymerization in the structure of melts with composition and are also listed in Table IV. The effects of FeO/SiO<sub>2</sub> ratios and the contents of CaO and Al<sub>2</sub>O<sub>3</sub> on the melt structures were evaluated by analyzing the calculated Q<sup>0</sup>/Q<sup>1</sup> ratios, providing insight into the distribution of the depolymerization of the silicate network. The samples with the same number but different letters can be compared to determine the effect of the FeO/SiO<sub>2</sub> ratio, showing that a higher FeO/SiO<sub>2</sub> ratio leads to higher Q<sup>0</sup>/Q<sup>1</sup> ratios and, thus, a more depolymerized melt. For example, the Q<sup>0</sup>/Q<sup>1</sup> ratios increased from 1.44 in 1L (low FeO/SiO<sub>2</sub> ratio) to 1.61 in 1H (high FeO/SiO<sub>2</sub> ratio), indicating that the 1H was

more depolymerized. The effect of the FeO/SiO<sub>2</sub> ratio on the depolymerization of the melt was in accordance with the study by Wang *et al.*<sup>[20]</sup> who studied the effect of Fe/SiO<sub>2</sub> and Fe<sub>2</sub>O<sub>3</sub> contents on viscous flow and slag structure. The study showed that increasing the Fe/SiO<sub>2</sub> ratio resulted in a less polymerized silicate network structure. FeO dissociates, forming Fe<sup>2+</sup> and free oxygen, breaking the Si–O–Si bond in the dimer structure and forming a melt richer in the completely depolymerized silicate monomer.

The Q<sup>0</sup>/Q<sup>1</sup> ratios can be correlated to the viscosity flow, where the samples with a higher FeO/SiO<sub>2</sub> had a significantly lower viscosity. These correlations confirm that a higher FeO/SiO<sub>2</sub> ratio leads to a more depolymerized melt, decreasing the viscosity. The bond between silicon and oxygen is covalent, which is relatively resistant to motions; breaking this bond means that the internal friction in the material decreases, leading to lower viscosity and activation energy.

Samples 3 and 4 (both L and H) have higher CaO contents than samples 1 and 2 (L and H). Table IV shows that the Q<sup>0</sup>/Q<sup>1</sup> ratios for samples with a high CaO content are significantly higher than those with a low CaO content. For example, 1L and 3L have the same composition besides the CaO content, which was higher in 3L. The Q<sup>0</sup>/Q<sup>1</sup> ratio increases from 1.44 in 1L to 1.97 in 3L, indicating that the melt was more depolymerized in 3L. This confirms that CaO behaves as a network-modifying oxide that depolymerizes the network structure. The effect of the depolymerization was also confirmed by the viscosity measurements, where the sample with higher CaO content had a lower viscosity.

For Al<sub>2</sub>O<sub>3</sub>, the content is higher in the even samples (2 and 4); when comparing the Q<sup>0</sup>/Q<sup>1</sup> ratios, it indicates that Al<sub>2</sub>O<sub>3</sub> (up to 5 at pct) has a minor effect on the structure of the melt. However, the Q<sup>0</sup>/Q<sup>1</sup> ratios were consistently higher when the Al<sub>2</sub>O<sub>3</sub> content was higher, indicating that the melt structure became depolymerized when the Al<sub>2</sub>O<sub>3</sub> content increased. The opposite trend was observed when comparing these data with the viscosity measurements. The viscosity was higher when the Al<sub>2</sub>O<sub>3</sub> content was higher, indicating that Al<sub>2</sub>O<sub>3</sub> acts as a network-forming oxide in the melt, which also was strengthened by comparing the (Al<sub>2</sub>O<sub>3</sub> + SiO<sub>2</sub>)/MO ratio with the viscosity. One explanation for the decreased Q<sup>0</sup>/Q<sup>1</sup> ratios may be because the increased content of Al<sub>2</sub>O<sub>3</sub> reduces the absolute amount of SiO<sub>2</sub> in the samples, thus decreasing the relative amount of [SiO<sub>4</sub>]<sup>4-</sup> in the melt.

The results demonstrated that the viscosity of the slag was significantly influenced by the FeO/SiO<sub>2</sub> ratio, CaO content, and Al<sub>2</sub>O<sub>3</sub> content. Higher FeO/SiO<sub>2</sub> ratios and increased CaO levels promoted depolymerization of the silicate network, as reflected in the relative area fractions of Q<sup>0</sup> and Q<sup>1</sup> units, leading to reduced viscosity. In contrast, higher Al<sub>2</sub>O<sub>3</sub> content increased viscosity due to the formation of AlO<sub>4</sub>-tetrahedron, enhancing the melt's polymerization. However, this was not verified in the Raman spectra and needs further study. These findings align with the study's objective of clarifying the

relationship between slag composition, ionic structure of the melts, and viscosity, offering critical insights for optimizing slag properties in industrial processes.

#### IV. CONCLUSIONS

The present study investigated the correlation between the ionic structure of the melt, polymerization degree, and the viscosity of FeO–SiO<sub>2</sub>–Al<sub>2</sub>O<sub>3</sub>–CaO–MgO–Cr<sub>2</sub>O<sub>3</sub> melts with varying compositions. The influence of the composition was estimated in a two-level full-factorial design of experiments with the factors Al<sub>2</sub>O<sub>3</sub> and CaO content and the FeO/SiO<sub>2</sub> ratio. Based on the experimental results, the following was concluded within the compositional window of the study:

- The viscosity was lower in the melts with higher NBO/T, which ranged from 1.68 to 2.92. A high FeO/SiO<sub>2</sub> ratio of 1.25 (at pct/at pct) and a high content of CaO (12 at pct) were beneficial for obtaining a low viscosity owing to the network-breaking characteristics of the components. At 1573 K, the viscosity of the melt with the lowest NBO/T (1.68) was 3.5 times higher than the melt with the highest NBO/T (2.92).
- Melts with lower NBO/T, FeO, and CaO content had higher activation energy. This highlights the correlation between the activation energy and the structure of the melt, where a more polymerized melt is more sensitive to temperature changes.
- The samples with a higher FeO/SiO<sub>2</sub> ratio (1.25 at pct/at pct) resulted in a more depolymerized melt according to the Q<sup>0</sup>/Q<sup>1</sup> than those with a lower ratio (1.08 at pct/at pct). The same correlation was seen when changing the CaO content from high to low. Both trends were consistent with the viscosity data, indicating that CaO and FeO act as network-breaking oxides depolymerizing [Si<sub>2</sub>O<sub>7</sub>]<sup>6-</sup> (Q<sup>1</sup>) into a melt richer in the monomer silicate structure (Q<sup>0</sup>, [SiO<sub>4</sub>]<sup>4-</sup>).
- A higher content of Al<sub>2</sub>O<sub>3</sub> (5 at pct) increased the viscosity and activation energy, indicating that Al<sub>2</sub>O<sub>3</sub> acts as a network-forming oxide in the melt. On the other hand, an increased Al<sub>2</sub>O<sub>3</sub> content resulted in a higher Q<sup>0</sup>/Q<sup>1</sup> ratio according to the results from the Raman spectra. This indicates that the current analysis does not fully explain the melt structure when the Al<sub>2</sub>O<sub>3</sub> content is higher.
- The relationship between the molar ratio of (Al<sub>2</sub>O<sub>3</sub> + SiO<sub>2</sub>)/MO and the viscosity showed a clear linear trend (R<sup>2</sup> of 0.97), where the viscosity increased with an increasing ratio, indicating that Al<sub>2</sub>O<sub>3</sub> and SiO<sub>2</sub> act as network-forming oxides polymerizing the melt.

In summary, this study highlights the correlation between slag composition, melt structure, and viscosity, providing a deeper understanding of how network-forming and -breaking oxides influence the polymerization degree and the resulting physical properties. The results from this study support the correlation

between ionic structure, NBO/T, and the molar ratio of  $(\text{Al}_2\text{O}_3 + \text{SiO}_2)/\text{MO}$ , where samples with a higher degree of polymerization resulted in a higher viscosity in the  $\text{FeO-SiO}_2\text{-Al}_2\text{O}_3\text{-CaO-MgO-Cr}_2\text{O}_3$  system.

## ACKNOWLEDGMENTS

The project was conducted within the Center for Advanced Mining and Metallurgy (CAMM) at Luleå University of Technology and financially supported by Boliden AB through Bolidenpaketet.

## FUNDING

Open access funding provided by Lulea University of Technology.

## CONFLICT OF INTEREST

The authors declare that they have no conflicts of interest.

## OPEN ACCESS

This article is licensed under a Creative Commons Attribution 4.0 International License, which permits use, sharing, adaptation, distribution and reproduction in any medium or format, as long as you give appropriate credit to the original author(s) and the source, provide a link to the Creative Commons licence, and indicate if changes were made. The images or other third party material in this article are included in the article's Creative Commons licence, unless indicated otherwise in a credit line to the material. If material is not included in the article's Creative Commons licence and your intended use is not permitted by statutory regulation or exceeds the permitted use, you will need to obtain permission directly from the copyright holder. To view a copy of this licence, visit <http://creativecommons.org/licenses/by/4.0/>.

## REFERENCES

- M. Kucharski, N.M. Stubina, and J.M. Toguri: *Can. Metall. Q.*, 1989, vol. 28, pp. 7–11.
- N.N. Viswanathan, F.Z. Ji, D. Sichen, and S. Seetharaman: *ISIJ Int.*, 2001, vol. 41, pp. 722–27.
- S. Nagraj, M. Chintinne, M. Guo, and B. Blanpain: *JOM*, 2022, vol. 74, pp. 274–82.
- I. Bellemans, J. Zietsman, and K. Verbeken: *J. Sustain. Metall.*, 2022, vol. 8, pp. 64–90.
- G.G. Stokes: *Trans. Cambridge Philos. Soc.*, 1850, vol. 9, pp. 75–129.
- I. Bellemans, E. De Wilde, N. Moeland, and K. Verbeken: *Adv. Col. Interf. Sci.*, 2018, vol. 255, pp. 47–63.
- M.E. Schlesinger, M.J. King, K.C. Sole, and W.G. Davenport: *Extractive Metallurgy of Copper*, 5th ed. Elsevier Ltd, Oxford, 2011.
- P.J. Mackey: *Can. Metall. Q.*, 1982, vol. 21(3), pp. 221–60.
- S. Mostaghel, C. Samuelsson, and B. Björkman: *Int. J. Miner. Metall. Mater.*, 2013, vol. 20, pp. 234–45.
- T.A. Utigard: *Scan. J. Metall.*, 1994, vol. 23, pp. 37–41.
- H. Shen and E. Forssberg: *Waste Manag.*, 2003, vol. 23, pp. 933–49.
- S. Northey, N. Haque, and G. Mudd: *J. Clean. Prod.*, 2013, vol. 40, pp. 118–28.
- K.C. Mills: *ISIJ Int.*, 1993, vol. 33, pp. 148–55.
- B. Mysen: *Eur. J. Mineral.*, 2003, vol. 15, pp. 781–802.
- B.O. Mysen and D. Virgo: in *Composition, Structure, and Properties of Mineral Matter: Concepts, Results, and Problems*, vol. 1, Springer, Berlin, Heidelberg, 1994, pp. 238–54.
- M. Chen, S. Raghunath, and B. Zhao: *Metall. Mater. Trans. B*, 2013, vol. 44B, pp. 506–15.
- Y. Shiraiishi, K. Ikeda, A. Tamura, and T. Saitô: *Trans. JIM*, 1977, vol. 19, pp. 267–74.
- G. Urbain, Y. Bottinga, and P. Richet: *Geochim. Cosmochim. Acta*, 1982, vol. 46, pp. 1061–72.
- H.-S. Park, S.S. Park, and I. Sohn: *Metall. Mater. Trans. B*, 2011, vol. 42B, pp. 692–99.
- B. Wang, H. Yang, Z. Jin, Z. Liu, and M. Zou: *Metals*, 2022, vol. 12, pp. 1–8.
- M. Mohri, Y. Sasaki, and K. Ishii: *ISIJ Int.*, 2001, vol. 41, pp. 410–15.
- J.R. Kim, Y.S. Lee, D.J. Min, S.M. Jung, and S.H. Yi: *ISIJ Int.*, 2004, vol. 44, pp. 1291–97.
- T. Li, C. Sun, S. Song, and Q. Wang: *Metals*, 2019, vol. 9, pp. 1–2.
- B. Wang, H. Yang, Z. Jin, T. Zheng, G. Chen, and Z. Dong: *JOM*, 2022, vol. 75, pp. 1221–29.
- Y.F. Chen, X.M. Lv, Z. De Pang, and X.W. Lv: *J. Iron Steel Rese. Int.*, 2020, vol. 27, pp. 1400–06.
- S. Mostaghel, T. Matsushita, C. Samuelsson, B. Björkman, and S. Seetharaman: *Miner. Process. Extr. Metall.*, 2013, vol. 122, pp. 42–48.
- M. Chen, S. Raghunath, and B. Zhao: *Metall. Mater. Trans. B*, 2013, vol. 44, pp. 820–27.
- T. Eguchi, N. Nishioka, and H. Takebe: *J. Sustain. Metall.*, 2023, vol. 9, pp. 1487–98.
- J. Hyun Park, D. Joon Min, and H. Seok Song: *Metall. Mater. Trans. B*, 2004, vol. 35, pp. 269–75.
- H. Doweidar: *J. Non-Cryst. Solids*, 1998, vol. 240, pp. 55–65.
- F.D. Richardson: *Physical Chemistry of Melts in Metallurgy*, vol. 1, London Press, London, 1974.
- A.C. Ducret and W.J. Rankin: *Scand. J. Metall.*, 2002, vol. 31, pp. 59–67.
- G.H. Kaiura, J.M. Toguri, and G. Marchant: *Can. Metall. Q.*, 1977, vol. 16(1), pp. 156–60.
- E. Selivanov, R. Gulyaeva, S. Istomin, V. Belyaev, S. Tyushnyakov, and A. Bykov: *Miner. Process. Extr. Metall.*, 2015, vol. 124(2), pp. 88–95.
- Y. Shen, J. Chong, Z. Huang, J. Tian, W. Zhang, X. Tang, W. Ding, and X. Du: *Materials*, 2019, pp. 1–16.
- Z. Yan, R.G. Reddy, X. Lv, Z. Pang, and C. Bai: *Metall. Mater. Trans. B*, 2019, vol. 50B, pp. 251–61.
- H. Zhang, L. Fu, J. Qi, and W. Xuan: *Metall. Mater. Trans. B*, 2019, vol. 50B, pp. 1852–61.
- J. Isaksson, A. Andersson, T. Vikström, A. Lennartsson, and C. Samuelsson: *J. Sustain. Metall.*, 2023, vol. 9, pp. 1378–89.
- A. Lennartsson, F. Engström, B. Björkman, and C. Samuelsson: *Can. Metall. Q.*, 2015, vol. 54(4), pp. 477–84.
- J. Isaksson, T. Vikström, A. Lennartsson, and C. Samuelsson: *Metals*, 2021, vol. 11, pp. 1–5.
- R. Roscoe: *Br. J. Appl. Phys.*, 1952, vol. 306, pp. 267–69.
- Y.L. Zhen, G.H. Zhang, and K.C. Chou: *Metall. Mater. Trans. B*, 2015, vol. 46, pp. 155–61.
- S. Wright, L. Zhang, S. Sun, and S. Jahanshahi: *Metall. Mater. Trans. B*, 2000, vol. 31B, pp. 97–104.
- B. Mysen and P. Richet: *Silicate Glasses and Melts*, 2nd ed. Elsevier, 2019.
- C.W. Bale, E. Béglise, P. Chartrand, S.A. Decterov, G. Eriksson, A.E. Gheribi, K. Hack, I.H. Jung, Y.B. Kang, J. Melançon, A.D. Pelton, S. Petersen, C. Robelin, J. Sangster, P. Spencer, and A.D. Van Ende: *Calphad*, 2016, vol. 54, pp. 35–53.
- A. Andersson, J. Isaksson, A. Lennartsson, and F. Engström: *J. Sustain. Metall.*, 2023, vol. 10, pp. 96–109.
- J. Isaksson, A. Andersson, A. Lennartsson, and C. Samuelsson: *Metall. Mater. Trans. B*, 2023, vol. 54, pp. 3526–41.
- B. Mysen, L. Finger, D. Virgo, and F. Seifert: *Am. Mineral.*, 1982, vol. 67, pp. 686–95.

49. M. Allibert, H. Gaye, J. Geiseler, D. Janke, B.J. Keene, D. Kirner, M. Kowalski, J. Lehmann, K. Mills, D. Neuschütz, R. Parra, C. Saint-Jours, P. Spencer, M. Susa, M. Tmar, and E. Woermann: *Slag Atlas*, 2nd ed. Verlag Stahleisen, Düsseldorf, 1995, p. 6.
50. L. Pargamin, C.H.P. Lupis, and P.A. Flinn: *Metall. Trans.*, 1972, vol. 3, pp. 2093–2105.
51. P. McMillan: *J. Non-Cryst. Solids*, 1983, vol. 55, pp. 221–42.
52. P.F. McMillan, W.T. Petuskey, B. Coté, D. Massiot, C. Landron, and J.-P. Coutures: *J. Non-Cryst. Solids*, 1996, vol. 195, pp. 261–71.
53. B.T. Poe, P.F. McMillan, C.A. Angell, and R.K. Sato: *Chem. Geol.*, 1992, vol. 96, pp. 333–49.
54. B.T. Poe, P.F. McMillan, B. Coté, D. Massiot, and J.P. Coutures: *J. Am. Ceram. Soc.*, 1994, vol. 77, pp. 1832–38.
55. L. Deng, S. Wang, Z. Zhang, Z. Li, R. Jia, F. Yun, H. Li, Y. Ma, and W. Wang: *Mater. Chem. Phys.*, 2020, vol. 251, pp. 1–9.
56. F.-Z. Ji, D. Sichen, and S. Seetharaman: *Metall. Mater. Trans. B*, 1997, vol. 28, pp. 827–34.
57. P. Atkins and J. de Paula: *Atkins Physical Chemistry*, 9th ed. Oxford University Press, 2009.
58. M. Flores-Favela, H. Pelaez-Ramirez, J. López-Rodriguez, A. Romero-Serrano, A. Hernández-Ramírez, A. Cruz-Ramírez, and I. Almaguer-Guzman: *Glass Phys. Chem.*, 2021, vol. 47, pp. 75–82.
59. J.S. Choi, T.J. Park, and D.J. Min: *J. Am. Ceram. Soc.*, 2021, vol. 104, pp. 140–56.
60. J.S. Choi, T.J. Park, D.J. Min, and I. Sohn: *J. Mater. Res. Technol.*, 2021, vol. 15, pp. 1382–94.
61. L. Deng, B. Yao, W. Lu, M. Zhang, H. Li, H. Chen, M. Zhao, Y. Du, M. Zhang, Y. Ma, and W. Wang: *J. Non-Cryst. Solid*, 2022, vol. 593, pp. 1–3.
62. T.S. Kim and J.H. Park: *J. Non-Cryst. Solids*, 2020, vol. 542, pp. 1–9.
63. H.-I. Kim and S.K. Lee: *Geochim. Cosmochim. Acta*, 2019, vol. 250, pp. 268–91.
64. K. Baert, W. Meulebroeck, H. Wouters, P. Cosyns, K. Nys, H. Thienpont, and H. Terryn: *J. Raman Spectrosc.*, 2011, vol. 42, pp. 1789–95.
65. B. Mysen, F. Seifert, and D. Virgo: *Am. Mineral.*, 1980, vol. 65, pp. 867–84.
66. M.T. Nayak and J.A.E. Desa: *J. Raman Spectrosc.*, 2018, vol. 49, pp. 1507–13.
67. S. Kashio, Y. Iguchi, T. Goto, Y. Nishina, and T. Fuwa: *Trans. ISIJ*, 1980, vol. 20, pp. 251–53.
68. J. Li, Q. Shu, and K. Chou: *ISIJ Int.*, 2014, vol. 54, pp. 721–27.
69. B. Mysen, D. Virgo, and C. Scarfe: *Am. Mineral.*, 1980, vol. 65, pp. 690–710.
70. J.H. Park: *ISIJ Int.*, 2012, vol. 52, pp. 1627–36.
71. Z. Wang, Q. Shu, and K. Chou: *ISIJ Int.*, 2011, vol. 51, pp. 1021–27.

**Publisher's Note** Springer Nature remains neutral with regard to jurisdictional claims in published maps and institutional affiliations.